Surface wave studies of the Greenland upper lithosphere using ambient seismic noise

Anatoli Levshin[1], Weisen Shen[2], Mikhail Barmin[1], and Michael Ritzwoller[1]

[1]Center for Imaging the Earth's Interior, Department of Physics, University of Colorado, Boulder, CO, USA
[2]Department of Earth and Planetary Sciences, Washington University in St Louis, St Louis, MO, USA

Corresponding author: Anatoli Levshin (levshin@colorado.edu)

ABSTRACT

Since 2009, the seismic stations as part of the Greenland Ice Sheet Monitoring Network (GLISN) have become available for broadband seismology on Greenland. Using this network, seismic surface waves can be exploited to study the structure of Greenland's upper lithosphere. In this paper we show some results of surface wave investigations utilizing the GLISN network. First, we measure the Rayleigh wave dispersion curves from ambient noise cross-correlations and use them to derive the information about the structure of the crust and uppermost mantle. We obtained ~190 reliable curves of Rayleigh wave phase and group velocities predominantly in the range of periods between 5 and 40 s. Then the two-dimensional tomography based on these data has been accomplished. It has the spatial resolution 300-450 km for latitudes between 64^o and 77^o N, going down to 650 km for northern latitudes and the southern tip of the island. Eventually, two types of 3D-inversion are applied to the set of tomographic maps in the period range 5-40 s. One of them used the sets of dispersion maps for 1^{o}x1^o grid obtained by bilinear interpolation for a regular set of periods. Other one used the surface wave dispersion information together with Rayleigh wave *H/V* ratios obtained for individual stations using teleseismic events. In both cases we applied Bayesian Monte Carlo inversion to infer the shear velocity structure of the crust and uppermost mantle of Greenland.

Key words: Ambient noise, Rayleigh waves, Crustal structure, Lithosphere structure, Greenland

1. Introduction

As the largest island on Earth, Greenland exhibits a wide variety of geological features, ranging from an early Archean shield to a large igneous province. A systematic and comprehensive investigation of its seismic structure, particularly the crust and uppermost mantle structure, provides important information to decipher the features' tectonic implications. However, the lack of open seismic data severely limited such investigation in the past. Most of studies were dedicated to receiver functions observed at the isolated stations (e.g., Dahl-Jensen *et a*l. 1998,

2003, 2012; Kumar *et al*. 2005). Studies of surface wave dispersion were done with few stations at the coast of Greenland (Gregersen 1970) or as a part of global tomographic studies (e.g. Artemieva *et al*. 2013, Kennett *et al*. 1995; Shapiro & Ritzwoller 2002; Ekström *et al*. 2007) with the spatial resolution for this region by the order 1000 km). The important exception was the study by (Darbyshire *et al*. 2004) in which authors have used data of the temporary network GLATIS with several broad-band stations in the middle part of island. Using observations of ~200 teleseismic events they obtained 45 inter-station Rayleigh phase velocity curves in period range 25-160 s. Inversion of these data provided new information about the structure of Greenland's lithosphere down to depth ~500 km. The spatial coverage of the island was still quite poor, especially at the North, and absence of data for shorter periods limited vertical resolution for the crust and upper mantle structure for the first 50 km.

Since 2009, the seismic stations of the Greenland Ice Sheet Monitoring Network (GLISN) have become available for broadband seismology on Greenland. Using this network, seismic surface waves can be exploited to study the structure of Greenland's upper lithosphere. Here we present results of surface wave investigations utilizing the GLISN network as our first attempt to pursue a comprehensive seismic model for Greenland. First, we measured the Rayleigh wave dispersion curves from the 3 years' stack of ambient noise cross-correlations using a manual FTAN program. We obtained about 190 reliable curves of Rayleigh wave phase and group velocities between different pairs of stations, predominantly in the range of periods between 5 and 40 s. We then applied two-dimensional tomography for the discreet set of periods to these data. Maps obtained are characterized by a spatial resolution of 300-450 km for latitudes between 64^o and 77^o N, going down to 650 km for northern latitudes and the southern tip of the island. Eventually two types of Bayesian Monte Carlo inversion were used to infer the shear velocity structure of the crust and uppermost mantle of Greenland. One type used sets of dispersion maps on a 1^ox1^o grid obtained by bilinear interpolation of tomographic maps for a regular set of periods. The other used the surface wave dispersion information and Rayleigh wave H/V ratios obtained for individual stations using teleseismic events.

2. GLISN project

The Greenland Ice Sheet Monitoring Network (GLISN, Clinton *et al*. 2014) started in 2009 by international collaboration of different countries: Canada, Denmark, France, Germany, Italy, Japan, Norway, Poland, South Korea, Switzerland, and the United States. This project provides real-time broadband seismological observations easily available through IRIS DMC. The project includes 33 stations in Greenland and around, including 19 stations in Greenland: 15 stations on the coasts and 4 in the middle part of the island. Other 14 stations situate on surrounding Greenland Arctic islands. In this study we analyze the data of all GLISN stations in Greenland (Denmark) and of station ALE (Alert, Ellesmere Island, Canada) which is separated from North Coast of Greenland by narrow shallow strait (see Figure 1 and Table 1). This network provides data convenient for surface wave tomography of the island.

Table 1 –GLISN stations used in this study

N	ID	Location	Longitude	Latitude	Seismic Sensors
1	ALE	Alert, Canada	-62.3500	82.5033	STS-1/STS-2
2	ANGG	Tasiilaq	-37.6371	65.6163	STS-2
3	DAG	Danmarkshavn	-18.6550	76.7713	STS-2
4	DBG	Daneborg	-20.2193	74.3071	STS-2
5	DY2G	Dye-2Raven Camp	-46.3094	66.4796	CMG-3T
6	ICESG	Ice South Station	-39.6474	69.0922	CMG-3T
7	ILULI	Ilulissat	-51.1048	69.2121	STS-2
8	IVI	Ivittuut	-48.1712	61.2058	STS-1
9	KULLO	Kullorsuaq	-57.2201	74.5805	STS-2
10	NEEM	NEEM drilling Camp	-51.0738	77.4447	CMG-3T
11	NOR	Station Nord	-16.6609	81.6047	STS-2
12	NRS	Narsarsuaq	-45.4188	61.1595	STS-2
13	NUUG	Nuugaatsiaq	-53.1996	71.5384	STS-2
14	NUUK	Nuuk	-51.6679	64.1838	STS-2
15	SCO	Ittoqqortoormiit	-21.9497	70.4856	STS-2
16	SFJD	Kangerlussuaq	-50.6208	66.9961	STS-1/STS-2
17	SOEG	Sødalen	-31.3755	68.2035	STS-2
18	SUMG	Summit	-38.4618	72.5742	STS-2
19	TULEG	Thule	-68.8237	76.5374	STS-2
20	UPNV	Upernavik	-56.1395	72.7829	T-240

3. Data and processing.

We collected continuous records of vertical channels from 20 mentioned above stations from IRIS Data Management Center for ~3 years of recording. As our goal was to extract surface wave information we processed the original data using the methodology described in detail at (Bensen *et al*. 2001). As result of this processing we obtained cross-correlations for all 190 pairs of stations. Paths between all pairs are shown in Figure 1b, and the histogram of the path lengths - in Figure 2. Path density is presented in Figure 3. We used Frequency-Time Analysis (FTAN) (e.g., Dziewonski *et al*. 1969; Levshin *et al*. 1972, 1989, 1992; Herrin & Goforth 1977; Russell *et al*. 1988; Ritzwoller & Levshin 1998; Levshin & Ritzwoller 2001) to extract from these cross-correlations the fundamental mode of Rayleigh waves and determine its phase and group velocity dispersion curves in the range of periods between 5 and 40 seconds.

Examples of FTAN diagrams of cross-correlation functions for 4 different pairs of stations with different path lengths are shown on Figure 4. Examples of cross-correlation functions and FTAN-filtered seismograms for two pairs of stations are presented on Figures 5a,b. Resulting phase and group velocity curves are shown on Figures 5c,d.

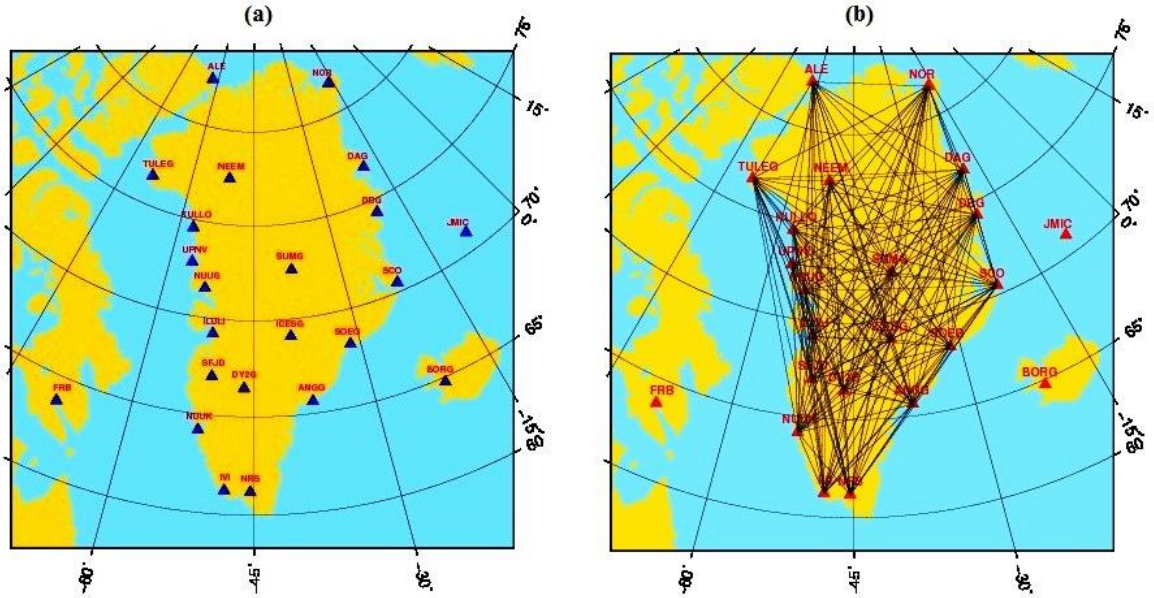

Figure 1. (a) GLISN stations; (b) inter-station paths used at this paper

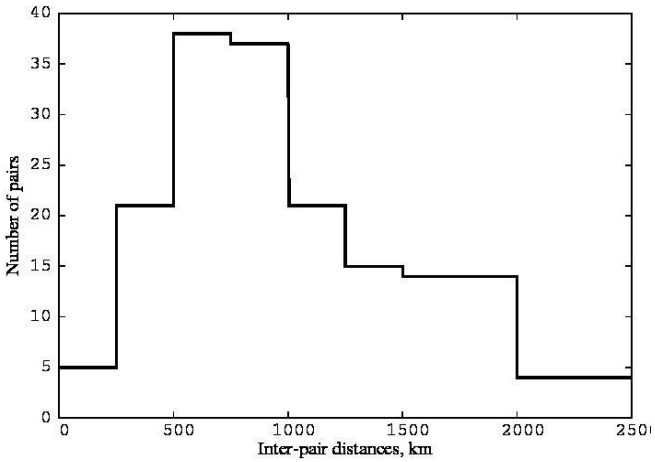

Figure 2. Histogram of inter-pair distances

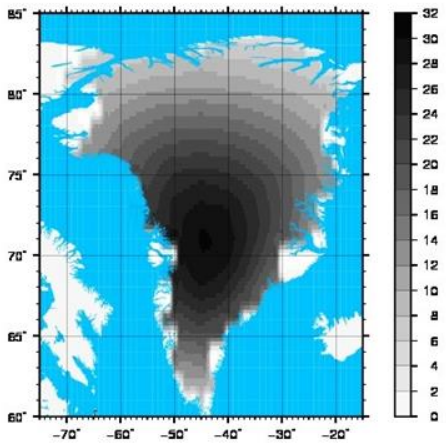

Figure 3. Path density: number of paths at 20s across an area 220x220 km2

We should note that FTAN-diagrams between coastal stations belonging to the same coast are often more complicated than ones for the paths crossing the inner parts of the island. It is due to multipathing along the shelf and internal parts of the island. For a few of these pairs the length of path is too short to get periods above 15 - 20s. Obtained dispersion curves for a set of periods T= 5-40s were discretized with an increment 1s. The obtained number of measurement at short and long periods varies depending on the length of pass (Figure 6).

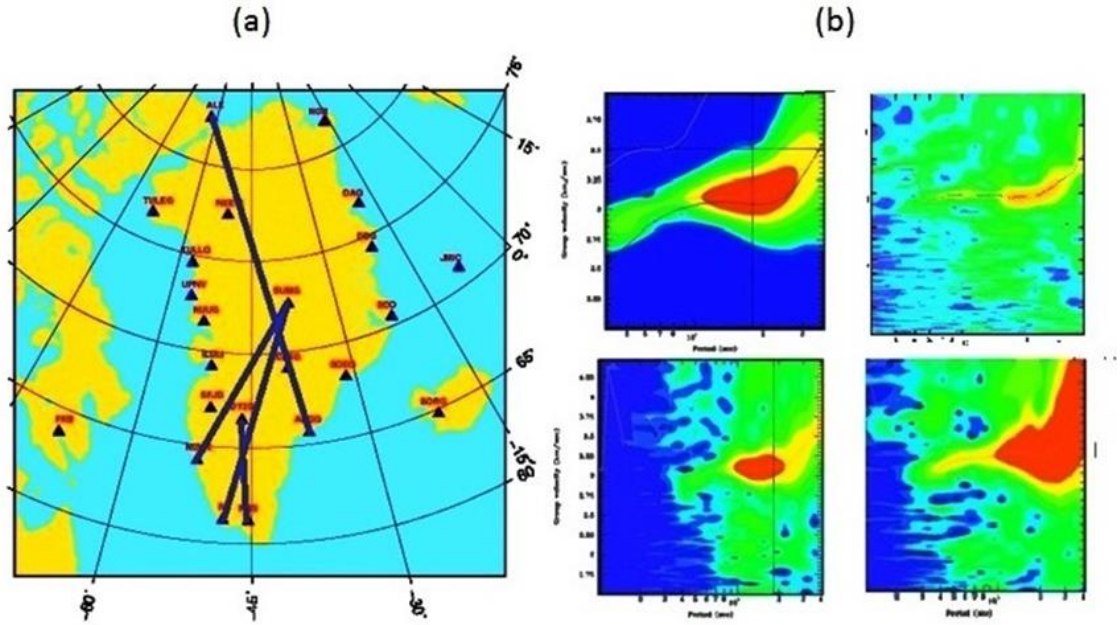

Figure 4. Examples of FTAN diagrams for 4 different pairs of stations: (a) Paths between stations; (b) FTAN diagrams for these paths.

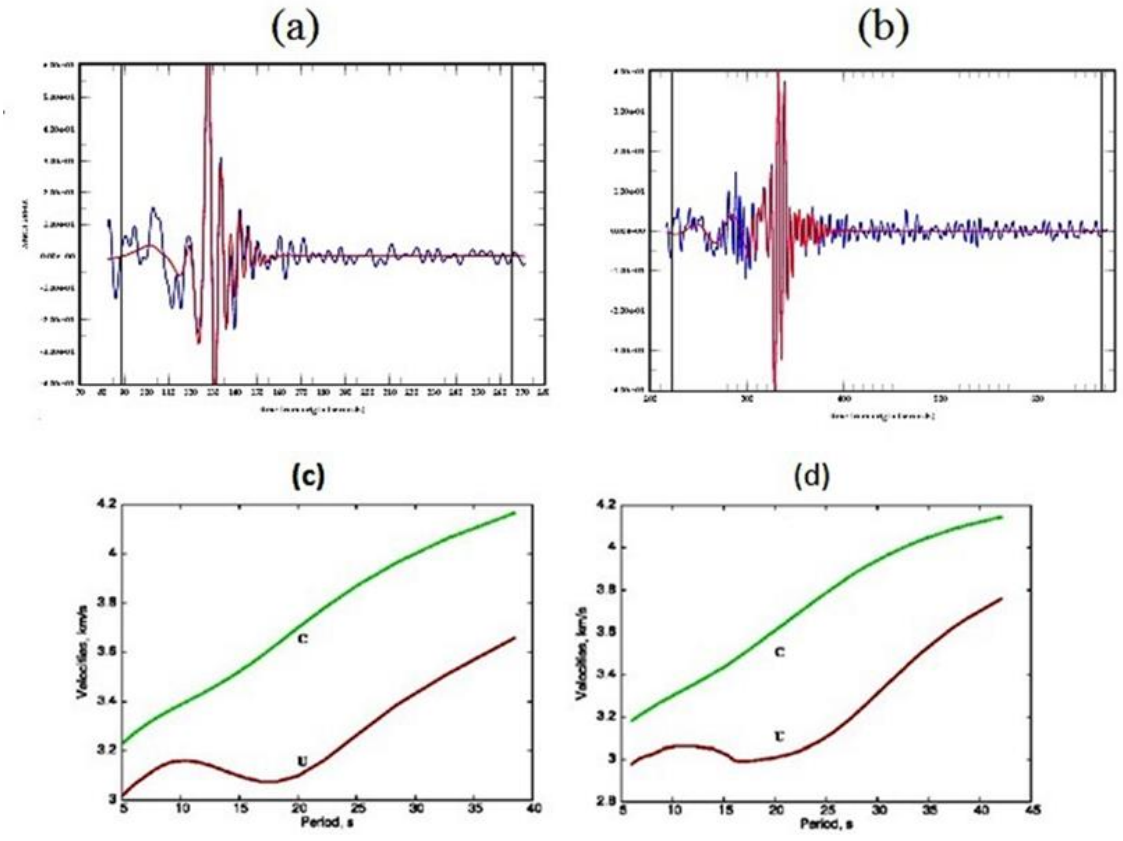

Figure 5. Examples of cross-correlation functions before and after FTAN-filtering: (a) ICESG- ANGG (400 km); (b) ICESG-NEEM (1000 km); (c) and (d) resulting phase and group velocities after FTAN.

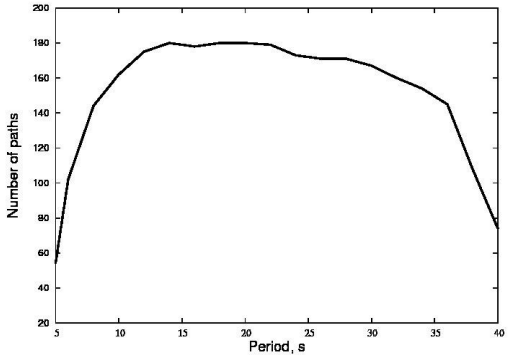

Figure 6. Number of paths after FTAN versus period.

4. Two-dimensional tomography

For tomographic inversion the territory of the island was covered by a grid with equatorial 2^{o} distances (220 km) between neighboring nodes. We applied so-called Gaussian tomographic inversion described in (Barmin *et al*. 2001; Ritzwoller *et al*. 2002). Spatial resolution at 20 s period, calculated as it is defined in (Barmin *et al*. 2001), is shown at Figure 7. We applied so-called Gaussian tomographic inversion described in (Barmin *et al*. 2001; Ritzwoller *et al*. 2002). Spatial resolution at 20 s period, calculated as it is defined in (Barmin *et al.* 2001), is shown at Figure 7.

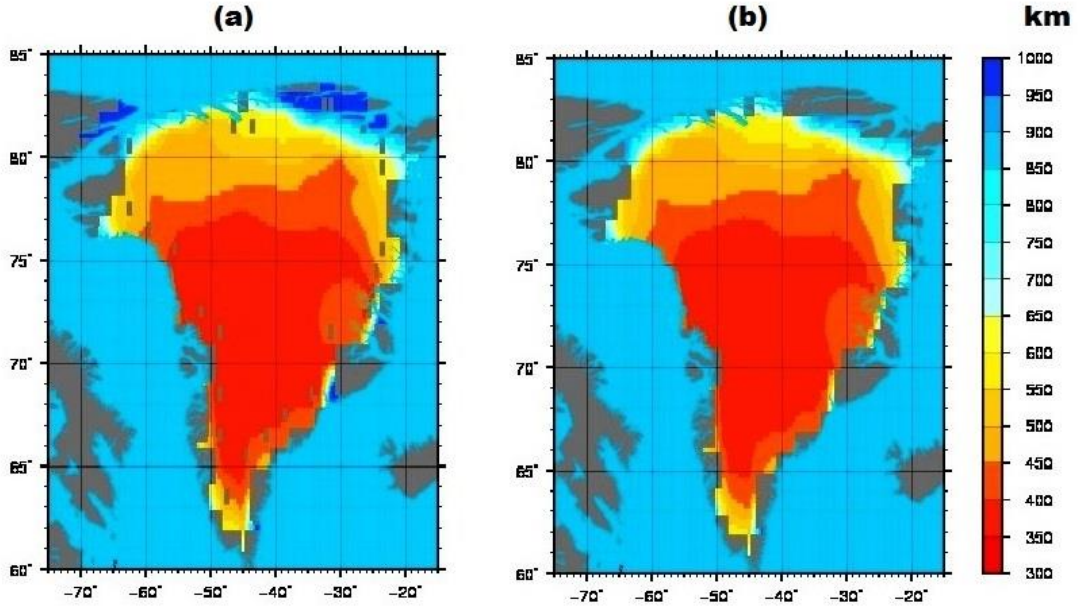

Figure 7. Spatial resolution at 20 s.: (a) Phase velocity; (b) Group velocity

The ranges of variations of phase and group velocities at different periods are given in Table 2.

Resulting inversion produced dispersion curves of phase and group velocities for each node in the mentioned above interval of periods. Set of dispersion curves obtained for grid points by 2-D tomography presented on Figure 8, resulting phase and group velocity maps - in Figure 9.

Table 2. Velocities of surface waves

Phase velocities						Group velocities				
T	*Cmin*	*Cmax*	*Caver*	*δCmin*	*δCmax*	*Umin*	*Umax*	*Uaver*	*δUmin*	*δUmax*
s	*km/s*	*km/s*	*km/s*	*%*	*%*	*km/s*	*km/s*	*km/s*	*%*	*%*
5	3.138	3.384	3.240	-3.15	4.44	2.829	3.251	3.021	-6.34	7.61
10	3.292	3.482	3.361	-2.05	3.60	2.869	3.226	3.100	-7.45	4.07
15	3.431	3.703	3.517	-2.44	5.29	2.873	3.195	3.070	-6.42	4.06
20	3.599	3.895	3.691	-2.50	5.52	2.991	3.406	3.114	-3.95	9.38
25	3.760	4.014	3.844	-2.20	4.41	3.090	3.598	3.220	-4.04	11.74
30	3.912	4.176	3.985	-1.84	4.79	3.152	3.641	3.361	-6.22	8.33
35	4.010	4.326	4.092	-2.00	5.72	3.339	3.649	3.501	-4.63	4.22
40	4.097	4.361	4.187	-2.14	4.16	3.438	3.772	3.659	-6.05	3.08

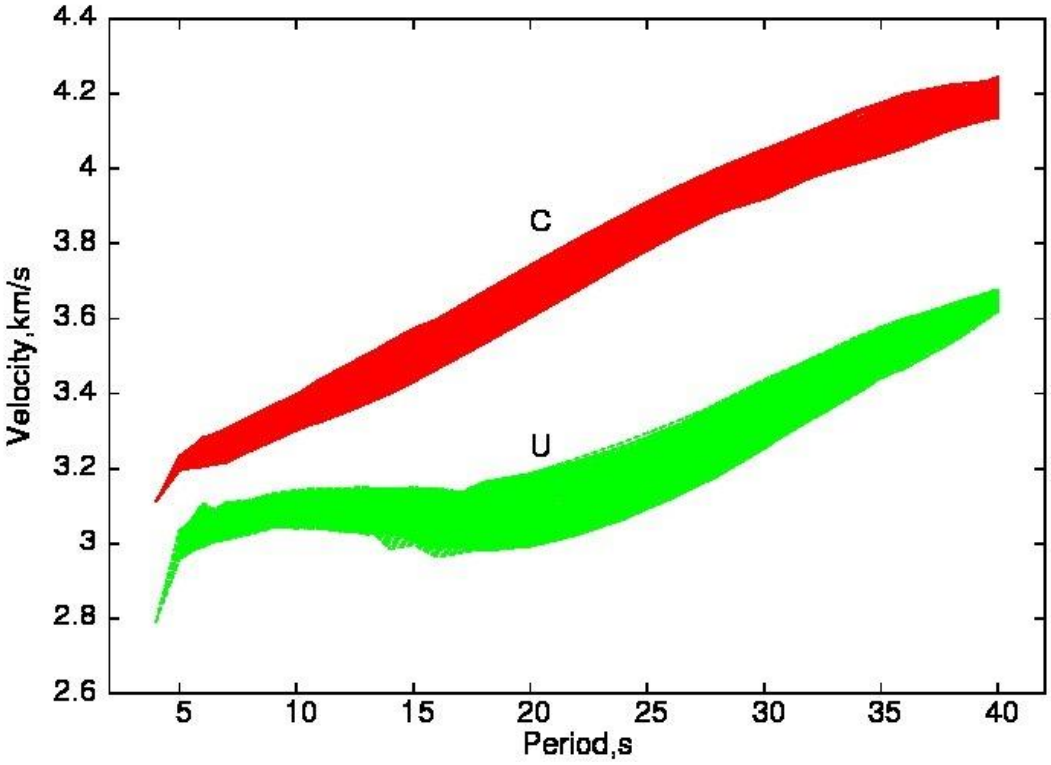

Figure 8. Set of dispersion curves of phase velocity (C) and group velocity (U) obtained for grid points by 2-D tomography

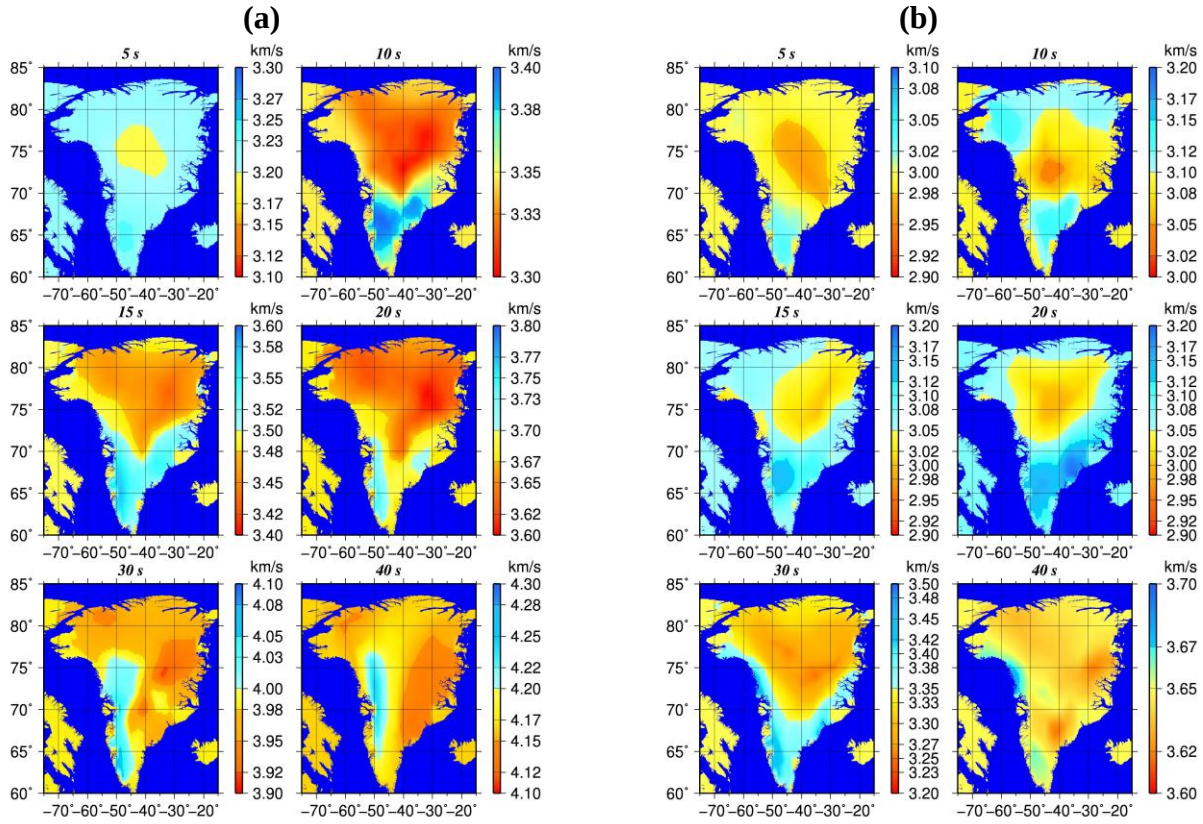

Figure 9. 2-D tomographic maps: (a) Phase velocity; (b) Group velocity

5. 3-D inversion

To build the 3-D shear velocity model of Greenland's upper lithosphere we applied methodology which is described in details by (Shen et al. 2013). This methodology is based on Bayesian Monte Carlo inversion used in many seismological applications. As we currently measure only Rayleigh wave dispersion, which is mostly sensitive to *Vsv*, the obtained model does not contain information about radial anisotropy.

The process of inversion includes several important stages.

The first stage is parametrization of the *Vs* model. The *Vs* model beneath each point of the grid is divided into four principal layers. The top layer is the ice which thickness and properties are supposed to be known (NASA Snow & Ice Center 2016). Below the ice is the sedimentary layer defined by three unknowns: layer thickness and *Vs* at the top and bottom of the layer with *Vs* increasing linearly with depth. The third layer is the crystalline crust, parameterized with five unknowns: four cubic B-splines and crustal thickness. Finally, there is the uppermost mantle layer, which is given by five cubic B-splines, yielding a total of 13 free parameters at each location. The thickness of the uppermost mantle layer is set so that the total thickness of all three layers is 200 km.

The second stage is definition of the reference model. This model consists of the 3-D model of (Shapiro & Ritzwoller 2002) for mantle's *Vsv*, crustal thickness and crustal shear wave speeds

from CRUST 2.0 (Bassin *et al*. 2000), and sedimentary thickness from (Mooney & Kaban 2010). Following (Shen *et al*. 2013b), the *Vp/Vs* ratio is set to be 2 for the sedimentary layer and 1.75 in the crystalline crust/upper mantle (consistent with a Poisson solid). Density is scaled from *Vp* by using results from (Christensen & Mooney 1995) in the crust and (Karato 1993) in the mantle. The *Q* model from the preliminary reference Earth model (Dziewonski & Anderson 1981) is used to apply the physical dispersion correction (Kanamori & Anderson 1977), and our resulting model is reduced to 1 s period.

The fourth stage is Bayesian Monte Carlo inversion of observed data in each point of the grid. Geophysical applications of Bayesian inference have been presented by (Tarantola & Valette 1982), (Mosegaard & Tarantola 1995) , (Mosegaard & Sambridge 2002), and (Sambridge & Mosegaard, 2002).

We refer to these works for technical details and present results of inversion of dispersion curves for two grid points (Figures 10, 11). The *Vs(z)* for model AK135 (Kennet 1995) is presented there for comparison with models obtained in result of inversion. The results of joint inversion of dispersion curves interpolated to the coordinates of stations and *H/V* ratios for two stations are presented in Figures 12, 13. As one can see the models obtained from two sets data are not significantly different.

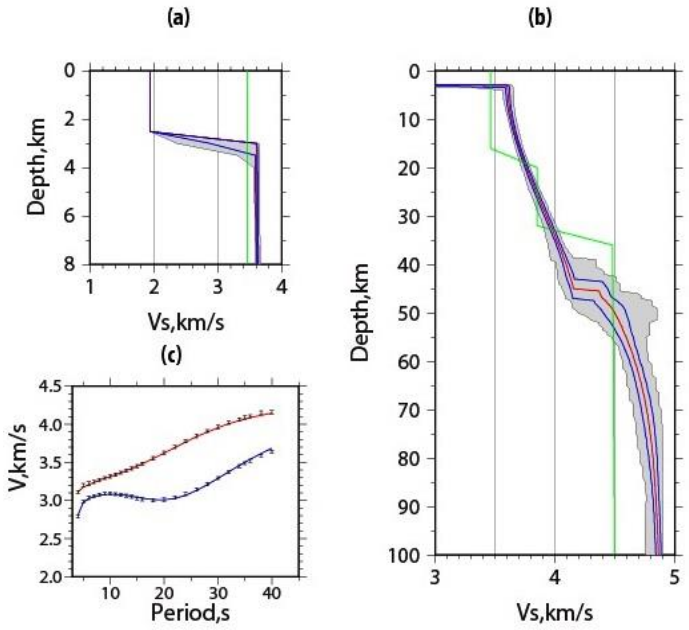

Figure 10. Example of 1D-inversion at the point 70^{o}N, 45^{o}W
(a,b) Ensemble of accepted models of the upper crust (a) and the upper lithosphere (b). The full width of the ensemble are presented as black lines enclosing a gray-shaded region, the 1$\boldsymbol{\sigma}$ ensemble is shown with red lines, and the average model is the black curve near the middle of the ensemble. Green line – AK135 model. (c) Rayleigh wave phase speed and group velocity curves corresponding the best fitting model (Fig.10a,b) shown by lines. Observed Rayleigh wave phase speed and group velocity curves presented as 1$\boldsymbol{\sigma}$ error bars.

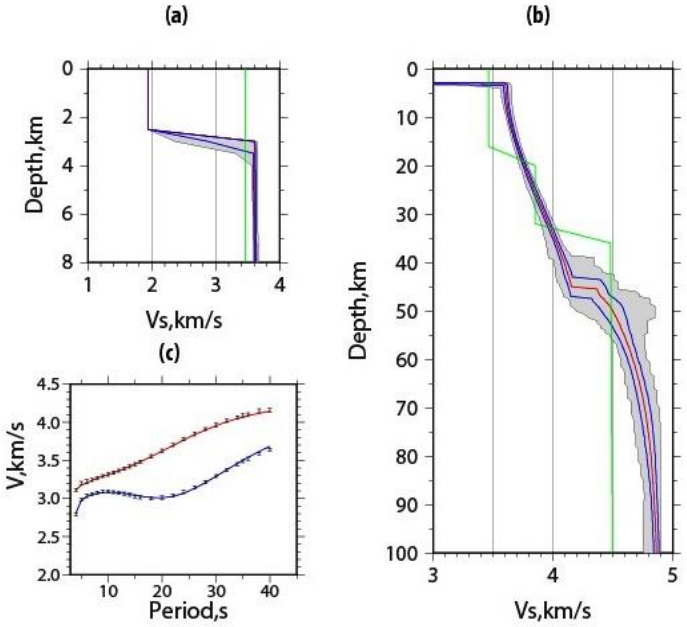

Figure 11. Example of 1D-inversion at the point 72°N, 37°W. The same legend as for Fig.10.

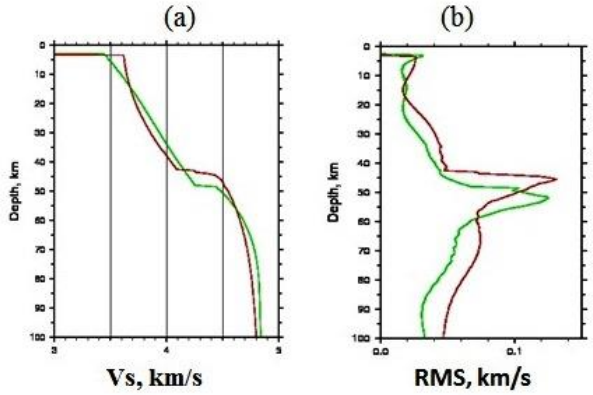

Figure 12. Comparison of 1D-inversions at the station SUMG using surface wave data with and without ellipticity (H/V) ratios. 1-D resulting *Vs*-model model; (b) RMS. Brown lines are for surface wave data only, green lines for surface wave data and ellipticity.

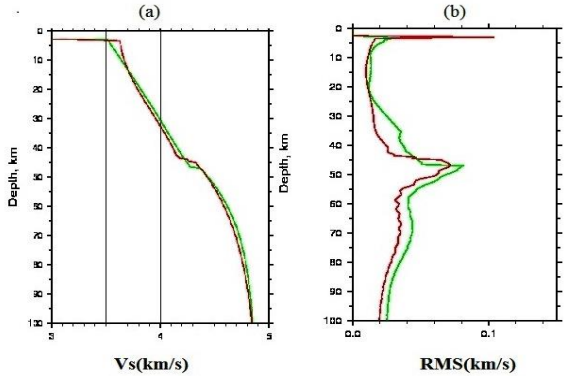

Figure 13. The same as at Fig.12 for station ICESG.

5. Results of inversion

The slices of Vs(λ,$\boldsymbol{\varphi}$) at two depths inside the crust are shown in Fig. 14. Relatively low velocities are at the Northern part of the island to the north of 70o latitude. Fig.15 presents the Moho depth and shear velocity directly under Moho. Depth of Moho varies from 37 km along coastal lines up to 43 km in the central region with undulations of around ±1 km. Shear wave speed under Moho is the highest between latitudes $70^o \div 75^o$.

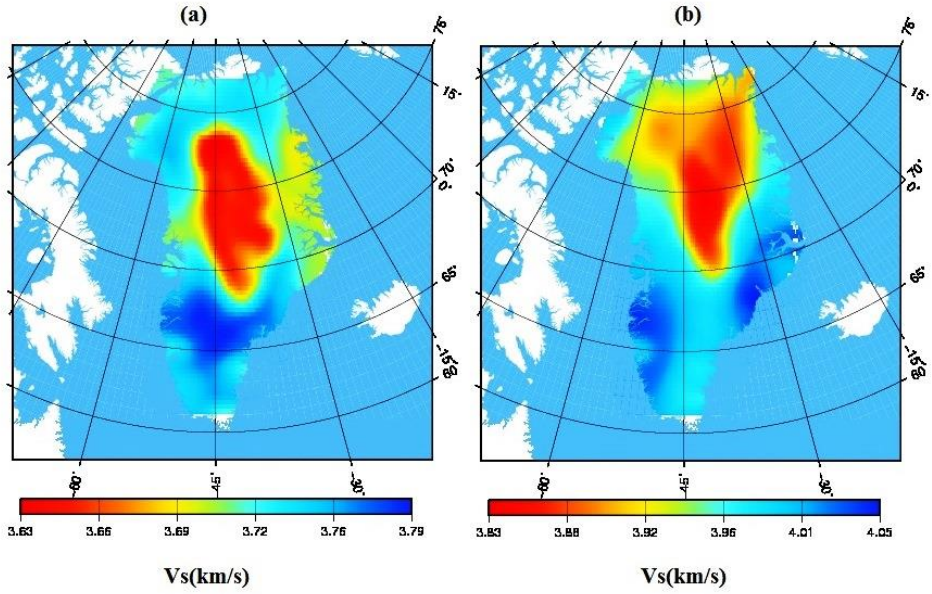

Figure 14. Shear velocities in the crust at the depth 10 km (a) and 30 km (b).

One can see significant differences in velocities in western and eastern parts of the island as divided by the longitude of ~45°W: western part is characterized by velocities ~0.15÷0.2 km/s higher than the eastern part. Ranges of lateral changes in *Vs* at different depths and in Moho depth are presented also in Table 3.

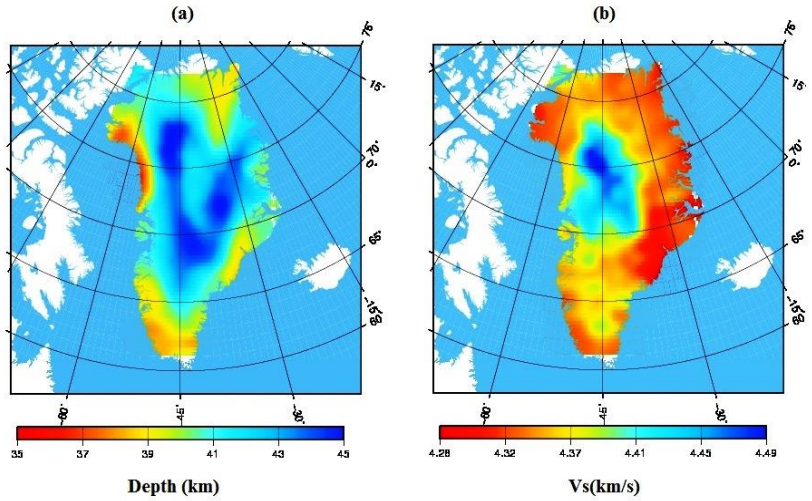

Figure 15. Depth of Moho boundary (a) and shear velocity along Moho (b).

Horizontal slices of *Vs* at the uppermost mantle on depths 80 and 100 km are shown in Figure 16.

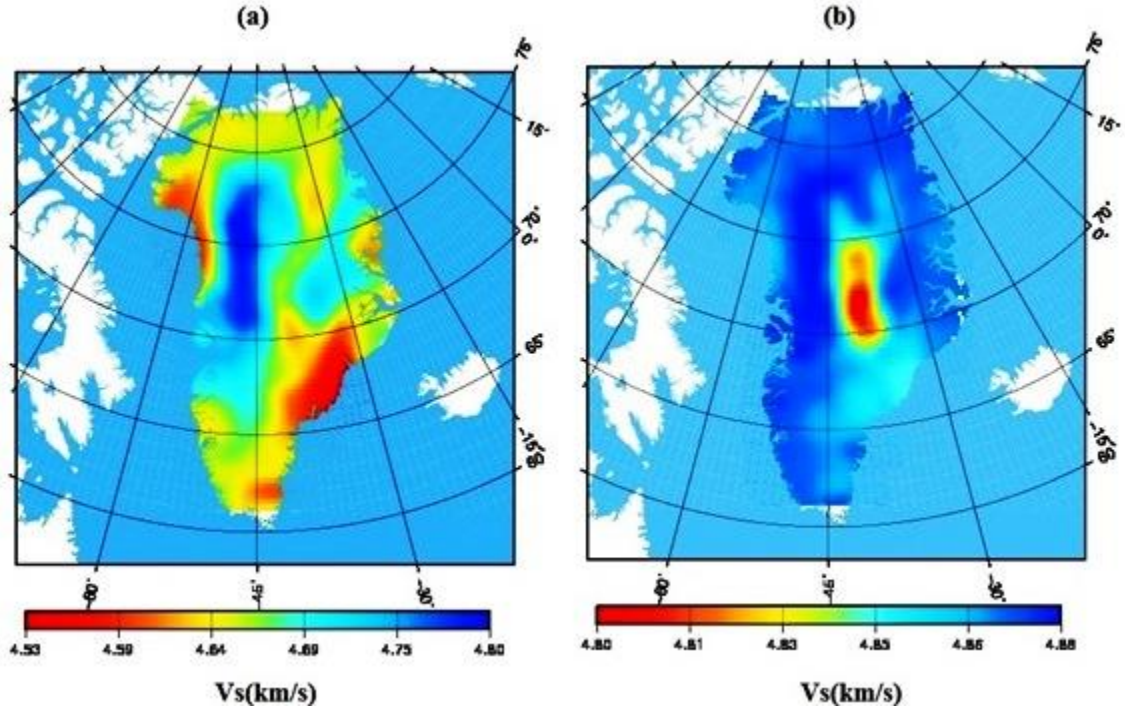

Figure 16. Shear velocities in the upper lithosphere: (a) at 20 km below Moho, (b) at the depth 100 km.

We demonstrate on Figures 18-20 vertical cross-sections of $Vs(z,\lambda,\boldsymbol{\varphi})$ along profiles shown on Figure 17. Meridional profile along $\lambda=45^{o}$W shows the lower crustal velocities at the depths 15-20 km in the central part of the island and higher upper mantle velocities at high latitudes ($\boldsymbol{\varphi}$ > 70^{o}N).

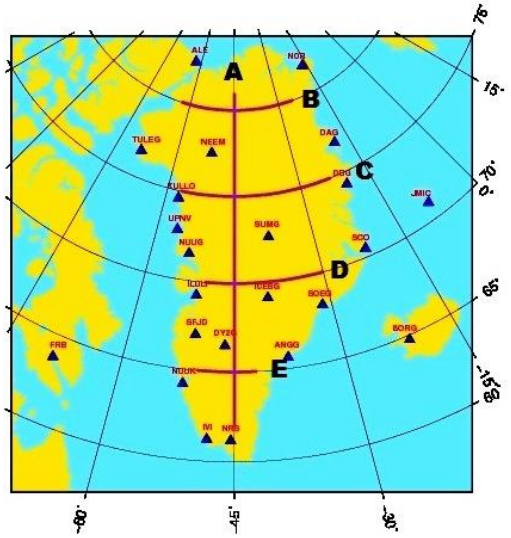

Figure 17. Vertical profiles across Greenland

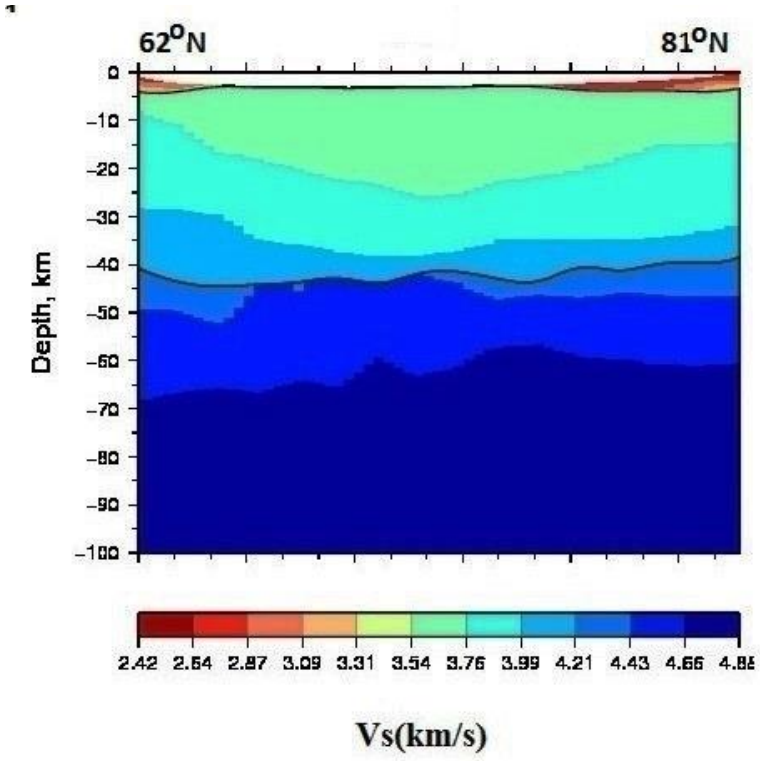

Figure 18. Vertical cross-section along meridional profile A (45°W)

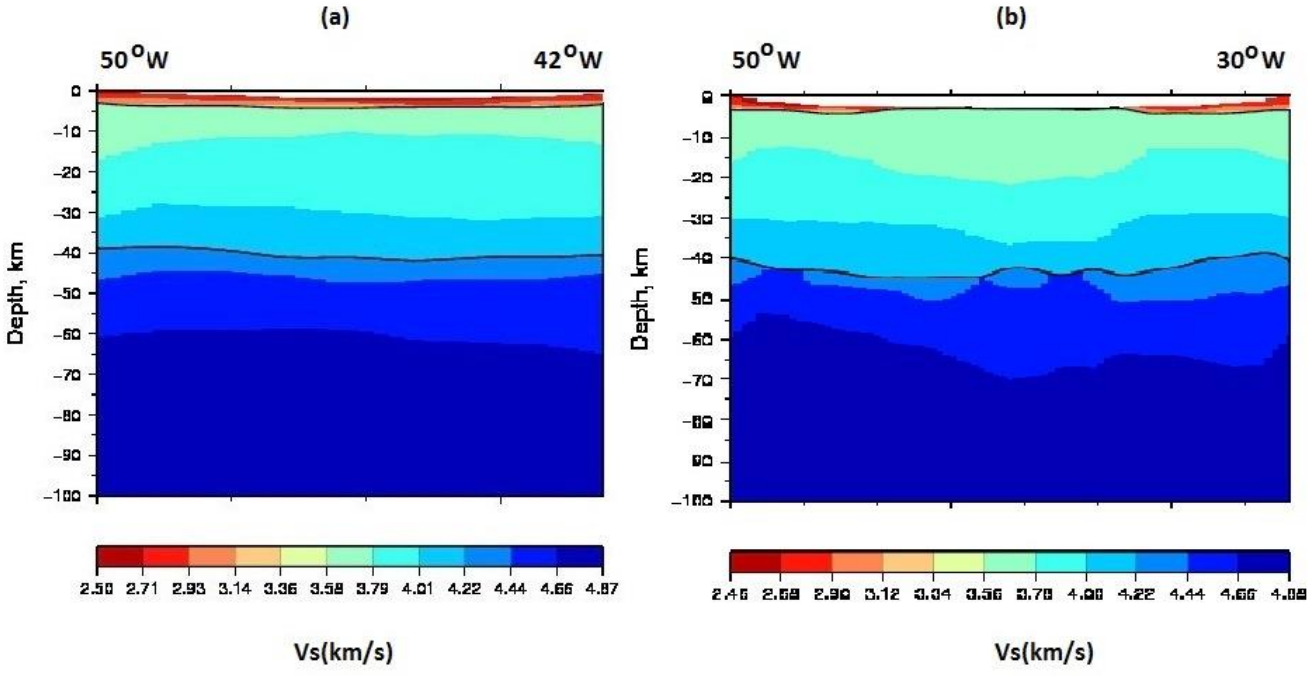

Figure 19. Vertical cross-sections along latitudinal profiles (a) E (65°N), (b) D (70°N)

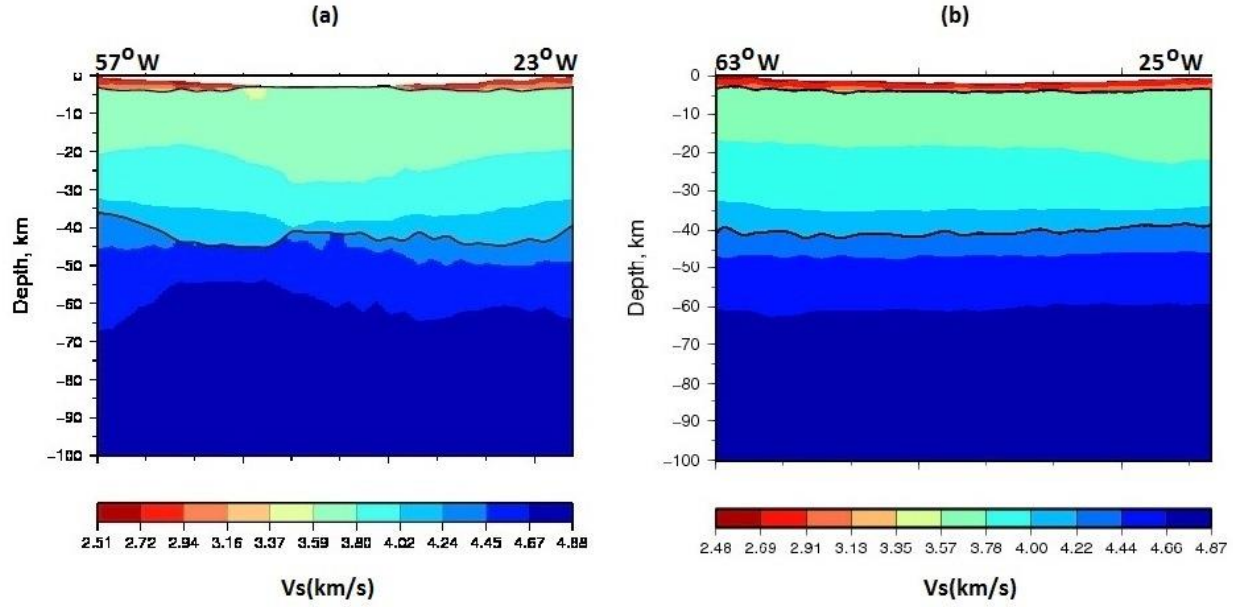

Figure 20. Vertical cross-sections along latitudinal profiles (a) C (75°N), (b) B (80°N)

Table 3. Range of parameters inside of the Greenland structure

Depth	*Vs aver*	*Vs min*	*Vs max*	*δVs min*	*δVs max*
km	*km/s*	*km/s*	*km/s*	*%*	*%*
10	3.71	3.62	3.79	-2.6	2.2
30	3.94	3.82	4.05	-3.0	3.0
Along Moho	4.37	4.28	4.56	-2.0	4.3
50	4.51	4.38	4.61	-2.7	2.3
70	4.75	4.66	4.85	-2.0	2.1
80	4.81	4.71	4.88	-1.9	1.4
100	4.86	4.78	4.89	-1.7	0.4
Depth to Moho	*H aver*	*H min*	*H max*	*δH min*	*δH max*
km	*km*	*km*	*km*	*%*	*%*
	41.6	35.1	46.6	-15.7	12.1

7. Conclusions

Analysis of several years of ambient noise records obtained by the GLISN stations provided new detailed information about structure of the crust and upper lithosphere of Greenland. Comparisons of the average crustal and upper lithosphere parameters of Greenland with predicted by one-dimensional Earth models (PREM, AK135, EUS) show that in average Greenland is characterized by more thick crust and higher velocities than one-dimensional Earth models. There are significant variations of Moho depth and shear velocity structure across Greenland in lateral directions in general agreement with previous less detailed studies. The

western part of the island basement is usually interpreted as of Archean origin has higher velocities than in the eastern part interpreted as of Proterozoic origin.
Further investigations may include: 1) joint interpretation of Love and Rayleigh wave data for determining anisotropic properties of the crust and upper lithosphere; 2) joint 3-D inversion of ambient noise and teleseismic data for obtaining more detailed data for lithosphere and asthenosphere including depths up to 300-400 km.

Acknowledgements

Authors are deeply thankful to participants and implementers of the GLISN project who opened the new page in studying the structure of the greatest island of the Earth.
The facilities of the IRIS Data Management System, and specifically the IRIS Data Management Center, were used to access the waveform and metadata required in this study. The IRIS DMS is funded through the National Science Foundation of the USA and specifically the GEO Directorate through the Instrumentation and Facilities Program of the National Science Foundation under Cooperative Agreement EAR-0552316.

References

Artemieva, I.M. and H.Thybo, 2013. EUNAseis: A seismic model for Moho and crustal structure in Europe, Greenland, and the North Atlantic region, Tectonophysics, 609, 97–153.

Barmin, M.P., M.H. Ritzwoller, and A.L. Levshin, 2001. A fast and reliable method for surface wave tomography, PAGEOPH, 158, n.8, 1351-1375.

Bassin, C., Laske, G. and Masters, G., The Current limits of resolution for surface wave tomography in North America, EOS Trans AGU, 81, F897, 2000.

Bensen, G.D., M.H. Ritzwoller, M.P. Barmin, A.L. Levshin, F. Lin, M.P. Moschetti, N.M. Shapiro and Y. Yang, 2007. Processing seismic ambient noise data to obtain reliable broad-band surface wave dispersion measurements, Geophys. J. Int., 169, 1239-1260.

Christensen, N.I. & Mooney, W.D., 1995. Seismic velocity structure and composition of the continental crust: a global view, J. geophys. Res., 100(B6), 9761–9788.

Clinton, J.F. *et al*., 2014. Seismic Network in Greenland Monitors Earth and Ice System, Eos, Vol. 95, No. 2, 13-24.

Dahl-Jensen, T., H. Thybo, J. Hopper, and M. Rosing, 1998. Crustal structure at the SE Greenland margin from wide-angle and normal incidence seismic data. Tectonophysics 288, 191–198.

Dahl-Jensen, T., T. B. Larsen, I. Woelbern, 2003. Depth to Moho in Greenland: Receiver-function analysis suggests two Proterozoic blocks in Greenland, Earth and Planetary Science Letters, 205, 379–393.

Dahl-Jensen, T., T.B. Larsen, P. Voss, 2012. Sedimentary thickness from Receiver Function analysis - a simple approach. Case study from North Greenland, Geophys. Res. Abstr.14 EGU2012-1649-1.

Darbyshire F., *et al*., 2004. A first detailed look at the Greenland lithosphere and upper mantle, using Rayleigh wave tomography. Geophys. J. Int., 158, 267-286, doi:10.1111/j1365-246X.2004.02316.x

Dziewonski, A.M., Bloch, S. & Landisman, M., 1969. A technique for the analysis of transient seismic signals, Bull. seism. Soc. Am., 59, 427–444.

Dziewonski, A. & Anderson, D., 1981. Preliminary reference Earth model, Phys. Earth planet. Inter., 25(4), 297–356.

Ekstrom, G., J. Tromp, and E. W. F. Larson, 1997. Measurements and global models of surface wave propagation, J. Geophys. Res.,102, 8137–8157.

Gregersen, S., 1970. Surface wave dispersion and crust structure in Greenland, Geophys. J. of the Royal Astronomical Society, 22, 22–39.

Herrin, E.E. & Goforth, T.T., 1977. Phase-matched filters: Application to the study of Rayleigh Waves, Bull. seism. Soc. Am., 67, 1259–1275.

Kanamori, H. & D. Anderson, 1977. Importance of physical dispersion in surface wave and free oscillation problems: review, Revs. Geophys. Space Phys., 15(1), 105–112.

Kanao, M., V.D. Suvorov, S. Toda, S. Tsuboi, 2015.Seismicity, structure and tectonics in the Arctic region, Geoscience Frontiers 6, 665-677.

Karato, S., 1993.Importance of anelasticity in the interpretation of seismic tomography, Geophys. Res. Lett., 20(15), 1623–1626, doi:10.1029/93GL01767.

Kennett, B. L. N., E. R. Engdahl, and R. Buland,1995. Constraints on seismic velocities in the Earth from travel times, Geophys. J. Int., 122, 108–124.

Kennett, B. , 1995. Approximations for surface–wave propagation in laterally varying media, Geophys .J. Int., 122, 470–478.

Köhler, A., C. Weidle, and V. Maupin, 2012. Crustal and uppermost mantle structure of southern Norway: results from surface wave analysis of ambient seismic noise and earthquake data. Geophys. J. Int. (2012) 191 (3): 1441-1456 doi:10.1111/j.1365-246X.2012.05698.x

Kumar P., R. Kind, W. Hanka, K. Wylegalla, Ch. Reigber, X. Yuan, I. Woelbern, P. Schwintzer, K. Fleming, T. Dahl-Jensen, T.B. Larsen, J. Schweitzer, K. Priestley, O. Gudmundsson, D. Wolf, 2005. The lithosphere–asthenosphere boundary in the North-West Atlantic region, Earth and Planetary Science Letters 236 (2005) 249– 257

Larsen T.B. *et al*., 2006. Earthquake seismology in Greenland – improved data with multiple applications, Geological Survey of Denmark and Greenland Bulletin 10, 57–60.

Laske, G. and G. Masters, A global digital map of sediment thickness, 1997, EOS Trans. AGU, 78, F483, 1997.

Levshin, A.L., Pisarenko, V.F., Pogrebinsky, G.A., 1972. On a frequency-time analysis of oscillations. Ann. Geophys., 28, 211-218.

Levshin, A.L., Ratnikova, L.I., Berger, J., 1992. Peculiarities of surface wave propagation across the Central Eurasia. Bull.Seism.Soc.Am., 82, 2464-2493.

Levshin A., Yanovskaya T., Lander A., Bukchin B., Barmin M., Ratnikova L., Its E., 1989. Seismic Surface Waves in a Laterally Inhomogeneous Earth, ed. Keilis-Borok V.I., Kluwer Oxford, UK, Norwell, MA.

Levshin, A.L. & Ritzwoller, M.H., 2001. Automated detection, extraction, and measurement of regional surface waves, Pure appl. Geophys., 158(8), 1531–1545.

Levshin A.L., M.H. Ritzwoller, M.P. Barmin, A. Villaseñor, C.A. Padgett, 2001. New constraints on the arctic crust and uppermost mantle: surface wave group velocities, Pn, and Sn, Physics of the Earth and Planetary Interiors 123 (2001) 185–204.

Mooney, W.D. & M.K. Kaban, 2010. The North American upper mantle: Density, composition, and evolution. Journal of Geophys. Res., 115, B12, doi:10.1029/2010JB000866

Mosegaard, K. & Tarantola, A., 1995. Monte Carlo sampling of solutions to inverse problems, J. geophys. Res., 100(B7), 12 431–12 447, doi:10.1029/94JB03097.

Mosegaard, K. & Sambridge, M., 2002. Monte Carlo analysis of inverse problems, Inverse Probl., 18, 29–54.

National Snow & Ice Data Center, 2016. Greenland 5 km DEM, Ice Thickness, and Bedrock Elevation Grids, NSIDC-0092.

Ritzwoller, M.H. & Levshin, A.L., 1998. Surface wave tomography of Eurasia:group velocities, J. geophys. Res., 103, 4839–4878.

Ritzwoller, M.H., N.M. Shapiro, M.P. Barmin, and A. L. Levshin, 2002.Global surface wave diffraction tomography, Geophys. J. Int., 107(B12), 2335.

Russell, D.W., Herrman, R.B. & Hwang, H., 1988. Application of frequency variable filters to surface wave amplitude analysis, Bull. seism. Soc. Am.,78, 339–354.

Sambridge,M., Mosegaard, K., 2002. MonteCarlo methods in geophysical inverse problems, Rev. Geophys., 40, 1–29.

Shapiro N.M., Ritzwoller M.H., 2002. Monte-Carlo inversion for a global shear-velocity model of the crust and upper mantle, Geophys. J. Int., 151, 88–105.

Shen, W., M.H. Ritzwoller, V. Schulte-Pelkum, F.-C. Lin, 2013. Joint inversion of surface wave dispersion and receiver functions: A Bayesian Monte-Carlo approach, Geophys. J. Int., 192, 807-836.

Tarantola, A. & Valette, B., 1982. Generalized nonlinear inverse problems solved using the least squares criterion, Rev. Geophys., 20(2), 219–232, doi:10.1029/RG020i002p00219.